Taylor & Francis
Taylor & Francis Group

Computer Methods in Biomechanics and Biomedical Engineering

ISSN: 1025-5842 (Print) 1476-8259 (Online) Journal homepage: http://www.tandfonline.com/loi/gcmb20

Collision rates for rare cell capture in periodic obstacle arrays strongly depend on density of cell suspension

I. Cimrák

To cite this article: I. Cimrák (2016): Collision rates for rare cell capture in periodic obstacle arrays strongly depend on density of cell suspension, Computer Methods in Biomechanics and Biomedical Engineering, DOI: 10.1080/10255842.2016.1165806

To link to this article: http://dx.doi.org/10.1080/10255842.2016.1165806

Published online: 29 Mar 2016.

Submit your article to this journal

View related articles

View Crossmark data

Full Terms & Conditions of access and use can be found at
http://www.tandfonline.com/action/journalInformation?journalCode=gcmb20

Download by: [Zilinska Univerzita v Ziline] **Date:** 04 April 2016, At: 03:16

COMPUTER METHODS IN BIOMECHANICS AND BIOMEDICAL ENGINEERING, 2016
http://dx.doi.org/10.1080/10255842.2016.1165806

Taylor & Francis
Taylor & Francis Group

Collision rates for rare cell capture in periodic obstacle arrays strongly depend on density of cell suspension

I. Cimrák

Cell-in-fluid Research Group, Faculty of Management Science and Informatics, University of Žilina, Žilina, Slovakia

ABSTRACT

Recently, computational modelling has been successfully used for determination of collision rates for rare cell capture in periodic obstacle arrays. The models were based on particle advection simulations where the cells were advected according to velocity field computed from two dimensional Navier–Stokes equations. This approach may be used under the assumption of very dilute cell suspensions where no mutual cell collisions occur. We use the object-in-fluid framework to demonstrate that even with low cell-to-fluid ratio, the optimal geometry of the obstacle array significantly changes. We show computational simulations for ratios of 3.5, 6.9 and 10.4% determining the optimal geometry of the periodic obstacle arrays. It was already previously demonstrated that cells in periodic obstacle arrays follow trajectories in two modes: the colliding mode and the zig–zag mode. The colliding mode maximizes the cell-obstacle collision frequency. Our simulations reveal that for dilute suspensions and for suspensions with cell-to-fluid ratio 3.5%, there is a range of column shifts for which the cells follow colliding trajectories. However we showed, that for 6.9 and 10.4%, the cells never follow colliding trajectories.

ARTICLE HISTORY
Received 2 September 2015
Accepted 10 March 2016

KEYWORDS
Rare cell capture; periodic obstacle arrays; collision rate; optimization; computational modelling

Downloaded by [Zilinska Univerzita v Ziline] at 03:16 04 April 2016

1. Introduction

The isolation and enrichment of rare cells from cell suspensions, such as circulating tumor cells from whole blood, belongs to important challenges with widespread biological and clinical applications. Microfluidic obstacle arrays as depicted in Figure 1(a) may be used with an antibody surface functionalization to both guide cells into contact with the capture surface and to facilitate adhesion.

To determine suitable geometry, a strategy called geometrically enhanced differential immunocapture (GEDI) has been used in Gleghorn et al. (2010), Santana et al. (2012), Huang et al. (2013) and Smith et al. (2014). Two dimensional Navier–Stokes equations were solved to obtain velocity profile of the fluid inside the device. Subsequently particle advection simulations were performed to advect cell positions inside the flow. This approach utilizes a one-way interaction between fluid and cells without cells affecting the flow.

Obtained data about cell trajectories, their positions, cell orientations, etc, were used to analyse different geometries. Gleghorn et al. (2013) and Smith et al. (2014) specified design parameters that induce high collision rates for all particles larger than a threshold size or selectively increase collision frequencies for a narrow range of particle sizes within a polydisperse population.

It is natural to expect that cell concentration influence the collision rate of cells with periodic obstacles in microfluidics. It is important to understand how the concentration affects the rate. One way to avoid this situation is to dilute the cell suspension to the level, that no cell–cell collisions occur. This however can lead to processing of larger volumes and thus to longer processing times. This is disadvantageous, since long processing time may have an adverse impact on viability of circulating tumour cells (Hong & Zu, 2013).

Other approach is to include the cell–cell collisions into the model. We further adopt this approach.

2. Methods

GEDI approach does not account for mutual cell collisions. We employ the object-in-fluid (OIF) framework introduced in Cimrák et al (2014) for full 3D computations of coupled fluid-cell interaction including cell–cell collisions.

In our approach, we use the lattice-Boltzmann method for the fluid. This method gives the velocity, density and other properties of the fluid in each time step on a fixed grid. The second component of the model governs mechano-elastic properties of biological cells and is based on immersed boundary (IB) method. Both components

CONTACT I. Cimrák ivan.cimrak@fri.uniza.sk

© 2016 Informa UK Limited, trading as Taylor & Francis Group

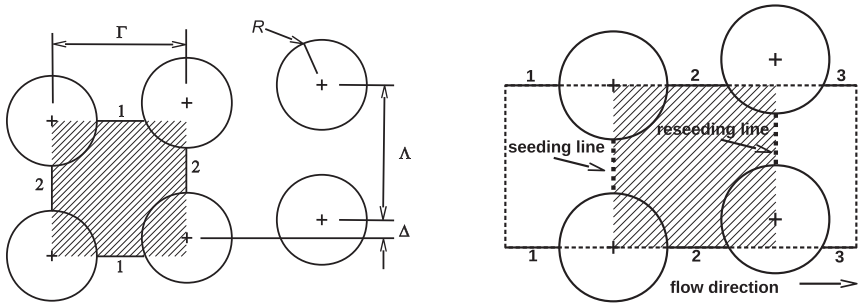

(a) **Periodic obstacle array. The velocity fields at lines 1 are identical due to periodicity. The same holds for lines 2.**

(b) Experiments A and B: cells at the reseeding line are reseeded to the seeding line

Figure 1. Schematics of periodic obstacle arrays and simulation setups. Notes: Simulated periodic block is indicated as dashed region. Rectangular computational domain is indicated by dashed line. Figures are drawn with $\Delta = 20\,\mu$m.

Downloaded by [Zilinska Univerzita v Ziline] at 03:16 04 April 2016

are coupled. The collision of cells are treated using repulsive potentials.

2.1. Lattice-Boltzmann method

This method is based on fictive particles. These particles perform consecutive propagations and collisions over a fixed 3D discrete cuboidal lattice. The unknown variable is the particle density function $n_i(x,t)$ defined for each lattice point x, discrete velocity vector e_i, and time t. We use the D3Q19 version of the LB method (three dimensions with 19 discrete directions e_i along the edges and diagonals of the lattice). The governing equations in the presence of external forces, are

$$\underbrace{n_i(x+e_i\delta_t, t+\delta_t) = n_i(x,t)}_{\textit{propagation}} \underbrace{- \frac{1}{\tau}(n_i(x,t) - n_i^{eq}(x,t))}_{\textit{collision}} + \underbrace{f_i(x,t)}_{\textit{external forces}} \tag{1}$$

where δ_t is the time step, τ denotes the relaxation time, n_i^{eq} is the equilibrium function, and f_i is the external force exerted on the fluid. We refer to Ahlrichs and Dunweg (1998) for details on the lattice-Boltzmann method. The velocity field u and the density of the fluid ρ are evaluated from

$$\rho(x,t) = \sum_i n_i(x,t) \qquad \text{and} \qquad \rho(x,t)u = \sum_i n_i(x,t)e_i.$$

2.2. IB method

Cell's membrane is covered by virtual points, so called IB points, linked together into a triangular mesh. Elastic properties of the cell membrane are represented with different types of force-like bonds between neighbouring mesh points. To take the mechano-elastic properties of the immersed objects into account, geometrical entities in this mesh (edges, faces, angles between two faces, …) are used to model stretching, bending, stiffness, and other properties of the boundary. They define forces according to the current shape of the immersed object that are exerted on IB points. These forces cause motion of the IB points according to the Newton's equation of motion

$$m\frac{\mathrm{d}^2 X_j}{\mathrm{d}t^2} = F_j \tag{2}$$

where m is the mass of the IB point, X_j is the position and F_j is the force exerted on the particular IB point j. The source of F_j is either from the above mentioned elasto-mechanical properties of the immersed object, or from the fluid-structure interaction.

2.3. Coupling of the lattice-Boltzmann method and the IB method

Equations (1) and (2) describe two different model components on two different meshes: the motion of the fluid and the motion of the immersed objects. For the coupling, we use an approach from Ahlrichs and Dunweg (1998) based on a drag force between the fluid and the IB points. The drag force exerted by the fluid on one IB point is proportional to the difference of the velocity v of the IB point and the fluid velocity u at the same position,

$$F = \xi(v - u).$$

Here ξ is a friction coefficient. The coupling is mutual so that the opposite force is exerted on the fluid.

2.4. Elasticity of the cells

The elasticity of the membrane is modeled by exerting forces on IB points on the boundary of the cell. Biological

Downloaded by [Zilinska Univerzita v Ziline] at 03:16 04 April 2016

membrane of a cell may have different elastic moduli for membrane stretching, bending, preservation of the surface and volume. For each modulus we use different force computation. For example, assume an elastic object has a relaxed shape, in which this object remains unless external forces are applied. In the relaxed shape, each local part of the surface has its area. In our model this part is modeled by a triangle with relaxed area S_0. If the cell deforms, this area changes to S and if it is larger than S_0, shrinking forces are exerted on the triangle vertices towards its centroid. If S is smaller than S_0, the forces have opposite sign and the surface is expanded.

Concrete expression for force calculation is

$$F_{\text{area}} = -k_{\text{area}} \frac{S - S_0}{\sqrt{S_0}},$$

where k_{area} is stiffness constant that is calibrated according to biological data. Further details on other formulae are presented in Jančigová and Cimrák (2015).

Gleghorn et al. (2013) consider LNCaP cancer cells that are stiffer than e.g. red blood cells. During their passage in periodic obstacle arrays they do not deform. Therefore in our experiments we considered the cells as elastic spheres with high stiffness. During all our simulations their longitudinal deformation did not exceeded 2%.

2.5. Mutual cell–cell interactions

The interactions between cells are treated by repulsive interactions. As soon as a part of cell membrane comes to close vicinity to other cell, repulsive forces are exerted on the corresponding mesh points of both membranes. These forces have cut-off radius less than 0.5 μm so that the forces act only if the mesh points from two different cells are closer than this threshold. The magnitude of the repulsive forces is set to be such that the two membranes never overlap.

3. Computational experiments

We performed two types of computational experiments. In the first experiment we focused on dilute suspensions where individual cells do not interfere and do not influence each others trajectories by mutual collisions. Dilute suspensions were thoroughly studied by Gleghorn et al. (2013) and Smith et al. (2014). We reproduced their results and so we showed that our model can capture simulation results as well as experimental results reported elsewhere. In the second experiment we focused on low and middle density cell suspensions. Here, mutual cell collisions are expected. We performed analysis of collision rates for cells for full range of offsets $\Delta \in (0, 75)$. Here we demonstrated that already at low densities of cell suspension, the optimal offsets completely differ from those obtained for very low cell densities.

Microfluidic channels containing periodic obstacle arrays are typically flat channels with width and length much larger than their height. We model channels containing 100 columns of obstacles. Because of the periodicity of obstacle positions we may consider only one periodic block that is repeating. In Figure 1(a) one such block is indicated as dashed region. The size of this block is $150 \times 150 \times 30\,\mu\text{m}$. In all experiments, $\Gamma = \Lambda = 150\,\mu\text{m}$, $R = 50\,\mu\text{m}$. The radius of cells equals $9\,\mu\text{m}$. The flow rate was set the same as in Gleghorn et al. (2013) to reproduce the results.

The OIF framework allows for setting periodic boundary conditions (BC) at the boundaries of the computational domain. For example, it is possible to set periodic BC at horizontal lines 1 in Figure 1(a) and thus the y-dimension of the computational domain is 150 μm. However, the OIF framework does not support shifted periodic BC. Our periodic block has vertical BC at lines 2 shifted with Δ in Figure 1. To resolve this issue we add additional channel length before and after the periodic box and thus our computational domain in x-direction has 325 μm. The obstacles were placed as indicated in Figure 1(b) with Δ varying. BC were periodic so that boundary parts 1, 2 and 3 coincide.

In an empty obstacle array the flow profile at seeding and reseeding lines would be the same. This way the fluid evolves into almost shifted-periodic flow profile at the seeding and reseeding lines. BC at inflow and outflow are set periodic.

3.1. Experiment A – dilute suspension

We uniformly seeded cells on the left inflow starting with cell touching the left-bottom obstacle, and ending with cell touching the left-top obstacle. Cell's position is given by the position of its center. Seeding positions all have the x-coordinate 0, the z-coordinate 15 and the y-coordinate ranges from 59 to 91, incremented by 0.5 μm. This results altogether in 65 seeding positions. For each seeding position we recorded the traces of the cell until its x-coordinate reaches Γ.

Given these 65 traces we can reconstruct the movement of the cell through the periodic obstacle array containing 100 columns. The y-coordinate of the cell at the end of the first trace defines the seeding position for the second trace taking into account the offset Δ. Subsequently, the y-coordinate at the end of the second trace defines the seeding position for the third trace, etc. For higher accuracy, we used the interpolation between the neighbouring traces.

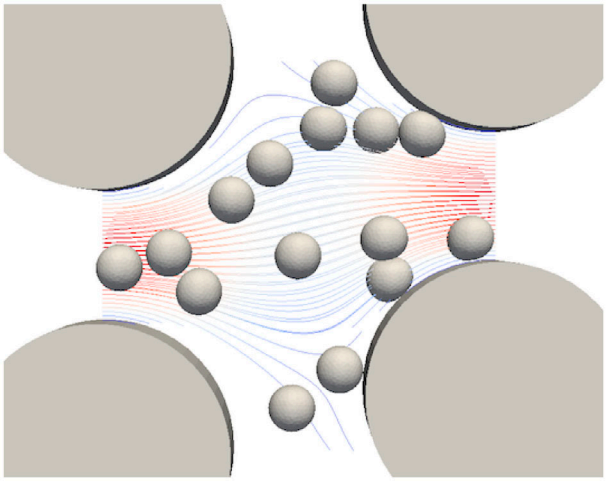

Figure 2. Streamlines of a fully evolved flow with 15 cells. Here $\Delta = 23\,\mu\text{m}$.

3.2. Experiment B – low to middle density suspension

Further we performed the set of simulations for three different cell counts: $n_1 = 5, n_2 = 10, n_3 = 15$ cells which corresponds to the cell-to-fluid fraction of 3.5, 6.9, and 10.4%.

For each cell density $n_i, i = 1, 2, 3$, we performed 76 long time simulations, one for each $\Delta = 0, 1, \ldots, 75\,\mu\text{m}$. For each Δ we randomly seeded corresponding number of cells between the seeding line and reseeding line, avoiding the obstacles. Then we let the flow evolve and we recorded the trajectories of individual cells. As soon as a cell reached reseeding line, we moved it back to the seeding line while preserving its distance from the bottom obstacles. For a snapshot of one such simulation see Figure (2). Movie with part of one of these long simulation is available as Supplementary material. The video shows simulation with $\Delta = 23\,\mu\text{m}$. The simulation was long enough so that each cell passed the reseeding line at least 50 times in order to get correct statistical data.

We are aware that the flow pattern between the obstacles at reseeding line is affected by the cells right before the reseeding of the cells. The flow at the seeding line however is not. This inaccuracy is negligible because the cells located at the reseeding line right before the reseeding follow the flow field and their velocity is almost identical compared to the velocity of the surrounding fluid in an empty channel, after the flow completely evolves. The relative difference stays under 1%.

This way we are able to simulate the movement of the cells through the periodic device. During the simulation, we recorded how many times a cell passed the obstacle, denoted by p^c_Δ, where $c = 1, 2, \ldots, n_i$ denotes the index of a cell for given $i, i = 1, 2, 3$. Also, we counted how many times a cell hits the obstacle, denoted by h^c_Δ. Collision frequency given in collisions per row (CpR) was calculated as fraction of hits and passes for each Δ resulting in $\text{CpR}_\Delta = \frac{\sum_{c=0}^{n_i} h^c_\Delta}{\sum_{c=0}^{n_i} p^c_\Delta}$.

4. Results

In experiment A, we obtained results depicted in Figure 3(a). Comparison with results depicted in Figure 8(a) (right) from Gleghorn et al. (2013) shows that both results are identical. In both figures we can see that most favorable geometry is at $\Delta/\Gamma_{\text{opt}} = 0.17$. With this experiment we demonstrated that our model can reproduce the results published elsewhere.

In the range $\Delta/\Gamma \in (0, 0.17)$ the CpR is monotonically increasing, reaching its maximum at $\Delta/\Gamma_{\text{opt}} = 0.17$, which is the optimal ratio for maximizing the CpR. In the range $\Delta/\Gamma \in (0.17, 0.42)$ CpR varies, but basically, it gets only four different values: 0.25, 0.33, 0.4, and 0.5. In the range $\Delta/\Gamma \in (0.42, 0.5)$ the values of CpR gradually decreases from 0.5 to 0.2.

From these results we may conclude that there are two modes for typical cell trajectories: the colliding mode and the zig–zag mode. In the colliding mode, $\Delta/\Gamma \in (0, 0.17)$ and the cells pass the obstacles along the top of the obstacle and are further diverted always up to pass again along the top of the next obstacle (with exception of very few passes in the beginning of their trajectory through the obstacle array). In the zig–zag mode, $\Delta/\Gamma \in (0.17, 0.5)$ and the cells are sometimes diverted up to pass along the top of the next obstacle and sometimes are diverted down to pass along the bottom of the next obstacle. The concrete interplay between how often they are diverted up and down determines the actual CpR.

In experiment B, we obtained completely different results depicted in Figures 3(b)–(d). With 5 cells in the channel, the cell-to-fluid ratio is only 3.5%. Even at such low cell density we obtained different optimal Δ/Γ. Although the shape of the curve at Figure 3(b) resembles the shape from Figure 3(a), the optimal value is shifted from 0.17 to $\Delta/\Gamma_{\text{opt}} = 0.12$.

This can be explained by looking more closely at cell trajectories. As we pointed out before, in dilute suspensions at optimal $\Delta/\Gamma = 0.17$, the trajectory of the cell is in colliding mode: cell touches the top of the obstacle after few passes. From then on, the cell follows the top of the obstacle and is further diverted up towards the top of the next obstacle. The size of the cell and the Δ ensure that the cell does not get below the next obstacle and that the trajectory do node change to zig–zag mode.

Downloaded by [Zilinska Univerzita v Ziline] at 03:16 04 April 2016

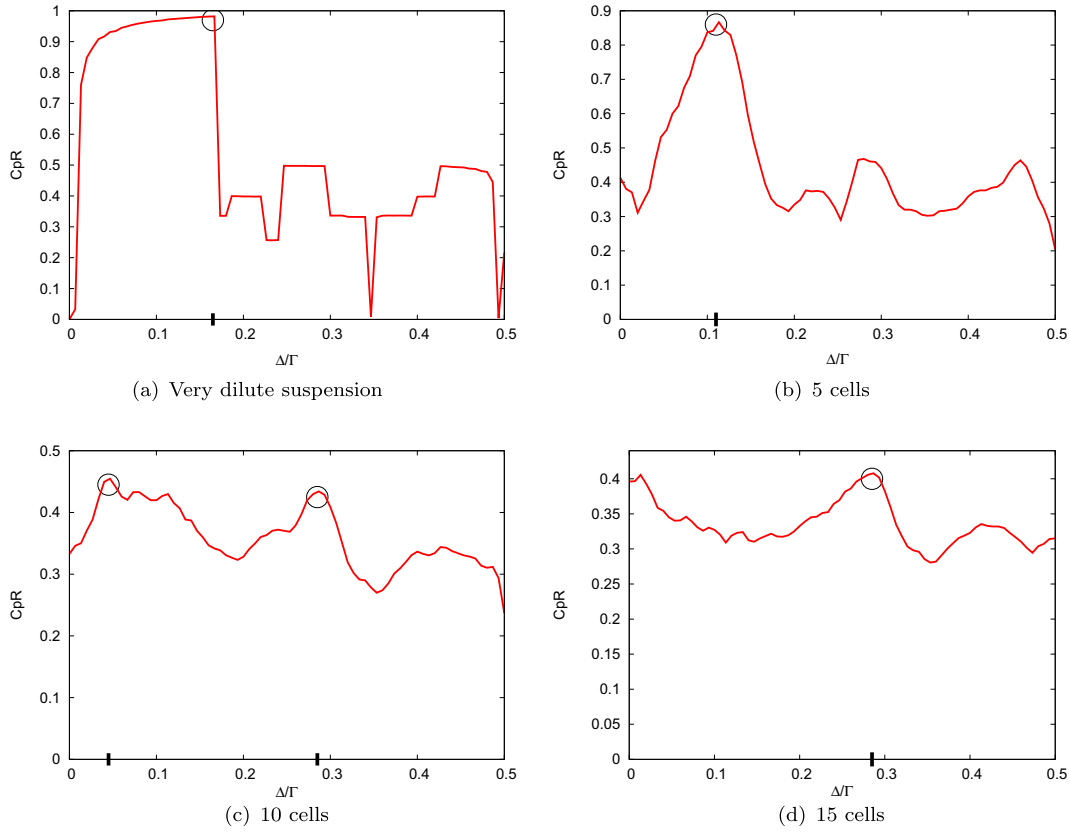

(a) Very dilute suspension (b) 5 cells

(c) 10 cells (d) 15 cells

Figure 3. Collision frequency for different cell counts. Optimal values of Δ/Γ and CpR are indicated with thick tic marks and circles.

In the experiment with cell-to-fluid ratio 3.5% and $\Delta/\Gamma = 0.17$, the cells sometimes collide with other cells and thus get pushed in out-of-streamline direction. This direction is either up or down. While the direction up does not influences whether cell remains in the colliding mode, the direction down can cause the cell to go below the obstacle and thus to switching to zig–zag trajectory. This subsequently decreases the CpR. To ensure that such occasional collision with out-of-streamline direction down does not divert the cell below the next obstacle, Δ must be lower. Therefore the optimal Δ/Γ ratio decreases for 3.5% hematocrit.

This phenomenon however is not present at even higher hematocrits. With 10 cells and 6.9% cell-to-fluid ratio, the situation is different, the highest CpR is reached for two values $\Delta/\Gamma_{opt} = 0.06$ and $\Delta/\Gamma_{opt} = 0.28$. With 15 cells and 10.4% cell-to-fluid ratio, there is single optimum at $\Delta/\Gamma_{opt} = 0.28$. We can clearly see from Figure 3 that maximal CpR reaches only 0.45 and 0.4, respectively.

This is caused by numerous cell–cell collisions causing the cells to be diverted below the obstacle too often. The cell simply never stays at the colliding mode for the whole course in the periodic obstacle array. From this behaviuor we can conclude that with higher cell-to-fluid ratio, cell trajectories are never in fully colliding mode. This is very important observation because it suggests that with higher hematocrits one can not expect too high CpR.

5. Discussion

We demonstrated that collision frequency in periodic obstacle arrays strongly depends on cell-to-fluid ratio. For very dilute suspensions where no mutual cell collisions occur, one can use particle advection simulations to determine optimal Δ/Γ. However for more detailed analysis for non-optimal values Δ/Γ, the OIF framework may give more accurate results.

For suspensions with cell-to-fluid ratio starting at 3.5%, one needs to account for mutual cell collisions. The simulations performed using the OIF framework showed significant differences when determining optimal Δ/Γ ratio. Not only the optimal value changes, but the optimum may be reached at multiple values, as shown in Figure 3(c).

The simulations further revealed that the cell trajectories in periodic obstacle arrays are in two modes: the colliding mode where the cell is always diverted up along the upper edge of the obstacles, and the zig–zag mode, where the cell is repeatedly diverted up and down.

Downloaded by [Zilinska Univerzita v Ziline] at 03:16 04 April 2016

We demonstrated that in dilute suspensions and in suspensions with cell-to-fluid ratio 3.5%, both modes occur and we determined the range of obstacle offset Δ / Γ for which the cells follow the colliding mode.

Finally we showed, that for suspensions with cell-to-fluid ratio 6.9 and 10.4%, the cells never enter the colliding mode and they always remain in zig–zag mode. This means that collision frequency rapidly decreases in these cases.

Disclosure statement

No potential conflict of interest was reported by the author.

Funding

This work was supported by the Marie-Sklodowska-Curie Actions [grant number PCIG10-GA-2011-303580]; the Slovak Research and Development Agency [contract number APVV-0441-11].

ORCID

I. Cimrák http://orcid.org/0000-0002-0389-7891

References

Ahlrichs P, Dunweg B. 1998. Lattice-Boltzmann simulation of polymer-solvent systems. Int J Mod Phys C. 8:1429–1438.

Cimrák I, Gusenbauer M, Jančigová I. 2014. An ESPResSo implementation of elastic objects immersed in a fluid. Comput Phys Commun. 185:900–907.

Gleghorn JP, Pratt ED, Denning D, Liu H, Bander NH, Tagawa ST, Nanus DM, Giannakakou PA, Kirby BJ. 2010. Capture of circulating tumor cells from whole blood of prostate cancer patients using geometrically enhanced differential immunocapture (GEDI) and a prostate-specific antibody. Lab Chip. 10:27–29.

Gleghorn JP, Smith JP, Kirby BJ. 2013. Transport and collision dynamics in periodic asymmetric obstacle arrays: rational design of microfluidic rare-cell immunocapture devices. Phys Rev E. 88:032136.

Hong B, Zu Y. 2013. Detecting circulating tumor cells: current challenges and new trends. Theranostics. 3:377–394.

Huang C, Santana SM, Liu H, Bander NH, Hawkins BG, Kirby BJ. 2013. Characterization of a hybrid dielectrophoresis and immunocapture microfluidic system for cancer cell capture. Electrophoresis. 34:2970–2979. http://dx.doi.org/10.1002/elps.201300242

Jančigová I, Cimrák I. 2015. A novel approach with non-uniform force allocation for area preservation in spring network models1). AIP Conf Proc. 1648:210004. Available from: http://scitation.aip.org/content/aip/proceeding/aipcp/10.1063/1.4912489

Santana S, Liu H, Bander N, Gleghorn J, Kirby B. 2012. Immunocapture of prostate cancer cells by use of anti-psma antibodies in microdevices. Biomed Microdevices. 14:401–407.

Smith J, Lannin T, Syed Y, Santana S, Kirby B. 2014. Parametric control of collision rates and capture rates in geometrically enhanced differential immunocapture (GEDI) microfluidic devices for rare cell capture. Biomed Microdevices. 16:143–151.

Downloaded by [Zilinska Univerzita v Ziline] at 03:16 04 April 2016